SHEAR LOCALIZATION IN A SPHERE-IMPACTED ARMOR-GRADE BORON CARBIDE

J.C. LaSalvia[1], R.C. McCuiston[1], G. Fanchini[2], J.W. McCauley[1], M. Chhowalla[2], H.T. Miller[1], and D.E. MacKenzie[1]

[1]U.S. Army Research Laboratory, AMSRD-ARL-WM-MD, Aberdeen Proving Ground, MD 21005-5069
[2]Rutgers University, Materials Science and Engineering Department, 607 Taylor Road, Piscataway, NJ 08854

Three armor-grade boron carbide cylinders were previously impacted with cemented carbide spheres at velocities 103 m/s, 209 m/s, and 312 m/s, respectively. These cylinders were subsequently sectioned and metallographically prepared to reveal sub-surface damage as a function of impact velocity. Each cylinder exhibited severe cracking including radial, shallow lateral, ring, and Hertzian cone cracks. The shallow lateral cracks extended to the upper surface, allowing spallation of material surrounding the impact site. No Mescall zone (i.e. comminuted region) was observed immediately beneath the impact site. At the impact site, an intact truncated cone was observed for an impact velocity of 103 m/s, while at the higher impact velocities, erosion of the cone was observed. Examination of these eroded cones revealed intense cracking. Furthermore, at the highest impact velocity of 312 m/s, narrow bands, which appear consistent with shear localization, were observed. Characterization of the sub-surface damage and shear localization "bands" by field-emission scanning electron microscopy is presented. Preliminary micro-Raman spectroscopy of the shear localization "bands" is also included.

INTRODUCTION

Because of its sufficient hardness and low density, boron carbide (B_4C) is an attractive ceramic for lightweight armor technologies designed for defense against common armor-piercing small-caliber threats [1-2]. However, it is generally found that B_4C loses its performance edge against medium-caliber threats [3] and possibly more severe small-caliber threats [4]. The reason for this loss of performance efficiency is not known with absolute certainty.

Plate impact work on B_4C has provided measurement of the mechanical response to shock compression [5-9]. Particle velocity histories are significantly different than

those for ceramic variants of aluminum oxide (Al_2O_3), silicon carbide (SiC), and titanium diboride (TiB_2) [6]. According to Bourne et al.[7], the response is more analogous to an amorphous glass than a polycrystalline ceramic. This is interesting because when subjected to compression, amorphous materials such as metallic glasses are susceptible to shear localization [10-11]. This suggests the possibility that B_4C may also be prone shear localization when subjected to compression.

Recently, results from a number of studies have supported the notion that B_4C is prone to shear localization. In their work on the ballistic performance of B_4C-based armor targets against a small-caliber cemented carbide cored projectile, Moynihan et al.[12] encountered a "shatter-gap". Unlike the traditional shatter-gap phenomenon, this one did not appear to be associated with a transition from intact core penetration to fragmenting core penetration. Examination of B_4C fragment sizes below and above the shatter-gap revealed a difference in fragment size distributions. Fragments from both populations were examined by Chen et al.[13] using transmission electron microscopy (TEM). TEM examination revealed the presence of nanometer wide amorphous bands in the fragments above the shatter-gap. These amorphous bands were not present in the fragments below the shatter-gap[†]. Amorphization of B_4C was previously suggested, though not concluded, by Domnich et al.[14] based upon their nanoindentation/Raman spectroscopy study on B_4C. The change in intensity of the amorphous carbon (C) peaks in the Raman spectrum taken from within the indent was indicative of structural change. Subsequent TEM examination by Ge et al.[15] of in-situ indents in B_4C confirmed the presence of shear amorphization regions as well as comminution at the nano-scale. The energetic driving force for the formation of these amorphous bands was recently studied by Fanchini et al.[16]. Based on a Gibbs free-energy analysis of B_4C polytypes with different possible boron (B) and C arrangements, they concluded that the B_{12}(CCC) polytype (i.e. B_{12} icosahedra connected by C-C-C chains) possessed the lowest mechanical stability when subjected to high pressures. The collapse of this crystal structure leads to the formation of 2-3 nm bands along the (113) lattice plane which are composed of B_{12} icosahedra and amorphous C [16].

In an attempt to gain further insight into the mechanistic reasons why B_4C behaves differently from other ceramics under dynamic loading conditions, LaSalvia et al.[17-18] impacted SiC, TiB_2, B_4C, and WC cylinders with cemented carbide spheres at velocities ranging between 100 m/s and 500 m/s. For SiC and TiB_2, polished cross-sections revealed cone (shallow ring and Hertzian) cracks and a compressive damage region, commonly referred to as the Mescall zone, immediately beneath the impact site (see Figure 1a [17]). This is consistent with the damage observed in these ceramics

[†]While the results of Moynihan et al.[12] led to the observation of shear amorphization in B_4C, it is not certain that this is the mechanism responsible for the shatter-gap. Other work revealed that the shatter-gap is dependent on tile size which indicates a connection to fracture toughness.

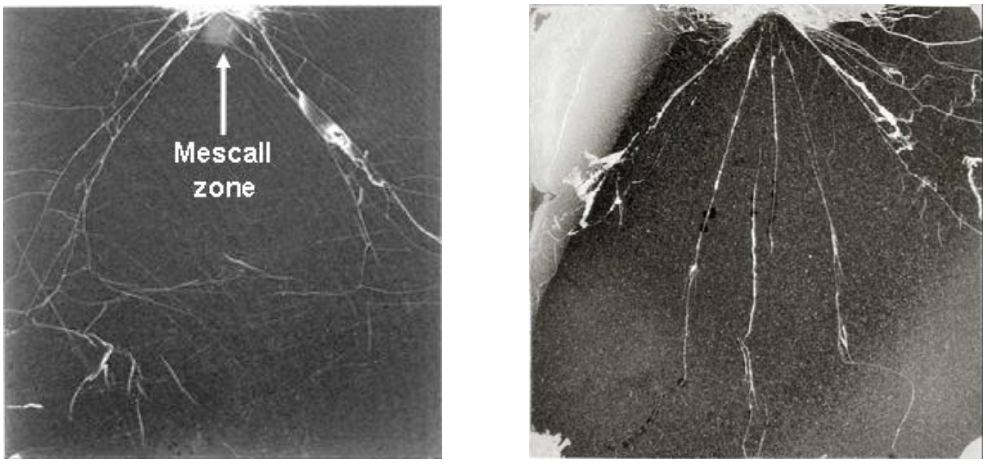

(a) (b)

Figure 1. Polished cross-sections of armor-grade (a) SiC [17] and (b) B_4C [18] showing damage resulting from the impact of WC spheres at 322 m/s and 312 m/s, respectively.

following their impact and recovery in interface defeat experiments conducted by Hauver et al.[19]. The resulting damage in the B_4C impacted at 312 m/s is shown in Figure 1b [18]. No Mescall zone is evident. Furthermore, the top surface of the truncated cone (bounded by top surface and main cone cracks) is 0.5 mm lower than the initial top surface. Closer examination at the top of the eroded truncated cone reveals fine cracking, as well as narrow "bands"[‡] of sub-micron fragments of B_4C as indicated by arrows in Figure 2 [18]. These bands are similar to the shear localization bands observed in Al_2O_3 and SiC by Meyers et al.[20] in their work involving explosively-driven collapse of thick-walled ceramic cylinders. Their work coupled with that of Ge et al.[15] strongly suggests that the bands shown in Figure 2 are shear localization bands. In an attempt to further study and gain better understanding of these bands, field-emission scanning electron microscopy (FE-SEM) and micro-Raman spectroscopy were utilized. General observations of characteristic damage features as a function of impact velocity and preliminary micro-Raman spectroscopy results are presented and discussed.

EXPERIMENTAL PROCEDURES

Solid cylinders of a armor-grade B_4C (25.4 mm x 25.4 mm), manufactured by BAE Advanced Ceramics Division, were impacted with 6.35 mm diameter cemented carbide

[‡]Quotations marks are used to indicate that the actual three-dimensional shape of these structures is unknown. Hereafter, simply referred to as bands.

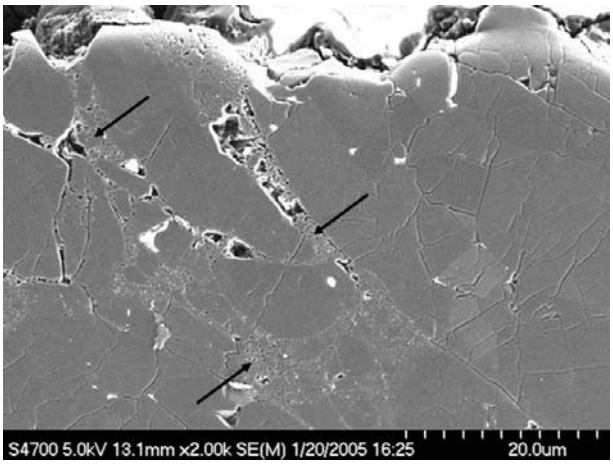

Figure 2 [18]. Cracking and micro-scale shear localization bands (arrows) of finely fragmented B_4C at the top surface of the eroded truncated cone.

Table 1. B_4C and WC-6Co Characteristics

Material	Density (g/cm^3)	Grain Size (μm)	Young's Modulus (GPa)	Poisson's ratio	Knoop Hardness @ 2 kg (GPa)	Fracture Toughness ($MPa*m^{1/2}$)	Tensile Strength (MPa)
B_4C	2.52	15	465	0.17	18.9	2.9	450
WC-6Co	15.00	2	629	0.21	-	-	3500

(tungsten carbide with six weight percent cobalt, i.e. WC-6Co) spheres at velocities between 100 m/s and 300 m/s. Several physical and mechanical characteristics for the B_4C and WC-6Co materials used in these experiments are listed in Table 1. The values for Young's modulus, Poisson's ratio, and tensile strength for WC-6Co were estimated based upon values obtained for a WC-6Co material with less than two percent porosity [21]. With the exception of the tensile strength estimate for the WC-6Co spheres, the measurement techniques used to determine them are described elsewhere [17]. In addition, details of the procedures for the sphere impact experiments are described by Normandia[22]. Impacted cylinders were sectioned adjacent to the impact site. The center of impact was revealed by carefully removing material through diamond grinding/polishing. Final polish was accomplished using colloidal silica. Polished cross-sections were examined using a Hitachi 4700 FE-SEM with back-scattered, secondary, and in-lense electron detectors, and energy-dispersive spectrometer (EDAX). Micro-Raman spectroscopy was conducted using a Renishaw InVia with 100 mW diode-based 785 nm wavelength near-IR laser with a spot size of 10 μm.

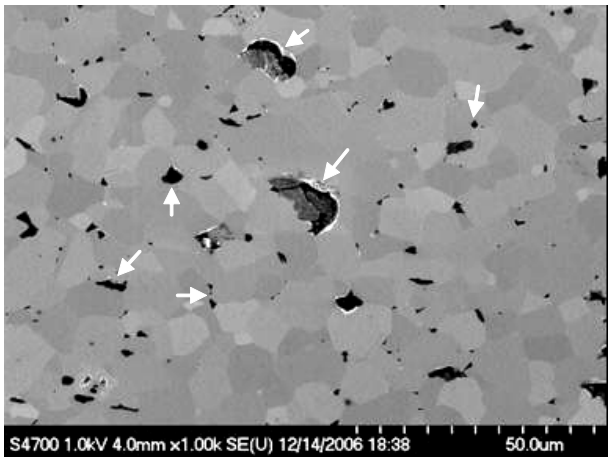

Figure 3. Microstructure of armor-grade B_4C. Dark features (arrows) are graphite particles.

RESULTS AND DISCUSSION

Figure 3 shows the microstructure of the armor-grade B_4C. As can be seen, the grain size is rather coarse, with a mean value of approximately 15 μm. Furthermore, the dark spots which appear to be porosity are actually graphite particles. The largest particles are greater than 10 μm in size. For the most part, these particles are intergranular. However, some of the smallest particles are intragranular.

The most noticeable feature observed in the B_4C cylinder impacted at 103 m/s was the intact truncated cone at the impact site as shown in Figure 4 [18]. The material surrounding this cone spalled off during unloading as a result of shallow lateral cracks intersecting with the top surface. The polished cross-section revealed multiple ring cracks surrounding the truncated cone and no Mescall zone.

At an impact velocity of 209 m/s, the truncated cone is no longer intact. Its height is below that of the initial impact surface. It is not known when this erosion took place, i.e. during loading, unloading, or both. A lateral crack near the top of the eroded cone was observed. This was most likely formed during unloading, strongly suggesting that the erosion occurred during loading. Cracking at the impact site and surrounding regions is more intense than at 103 m/s. It is possible that the erosion was simply due to the movement of this intensely cracked material. No shear localization bands were observed.

Figure 5 is a series of SEM micrographs taken from the polished cross-section of the eroded cone region for the cylinder impacted at 312 m/s. The boxes indicate the approximate locations where the subsequent images were taken. Intense cracking is clearly visible in Figures 5(a), (b), and (c). At sufficiently high magnification, shear

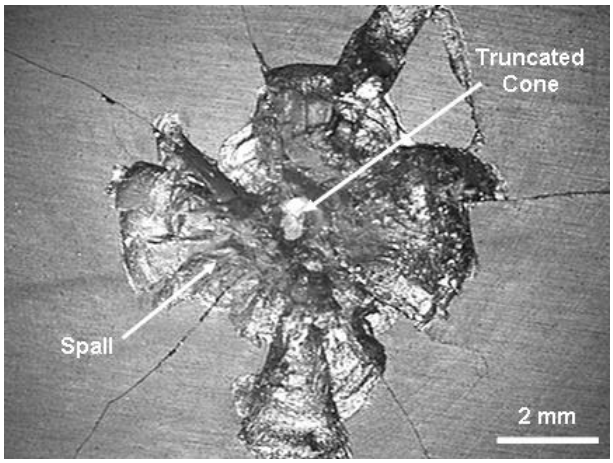

Figure 4 [18]. Impact site for impact velocity of 103 m/s.

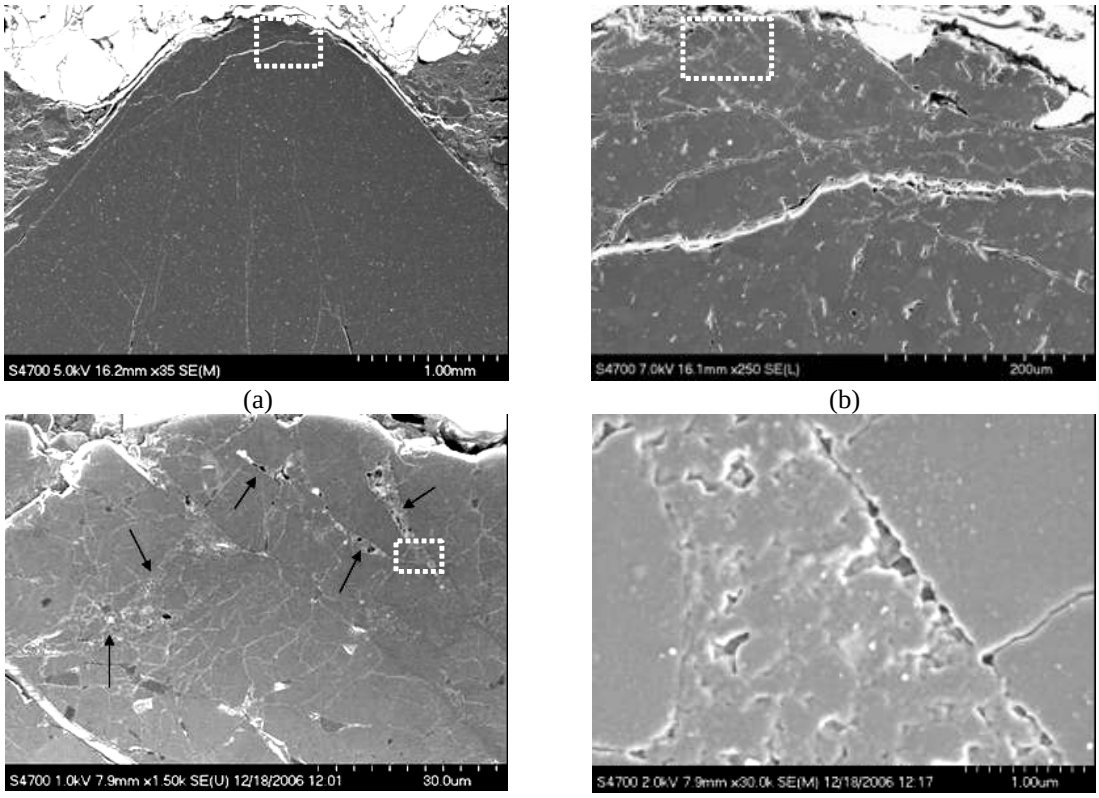

(a) (b) (c) (d)

Figure 5. SEM micrographs from cylinder impacted at 312 m/s. Boxes designate approximate locations for subsequent images. (a) Eroded cone region. (b) Top of eroded cone. (c) Shear localization bands at top of eroded cone (arrows). (d) B_4C particles within shear localization bands.

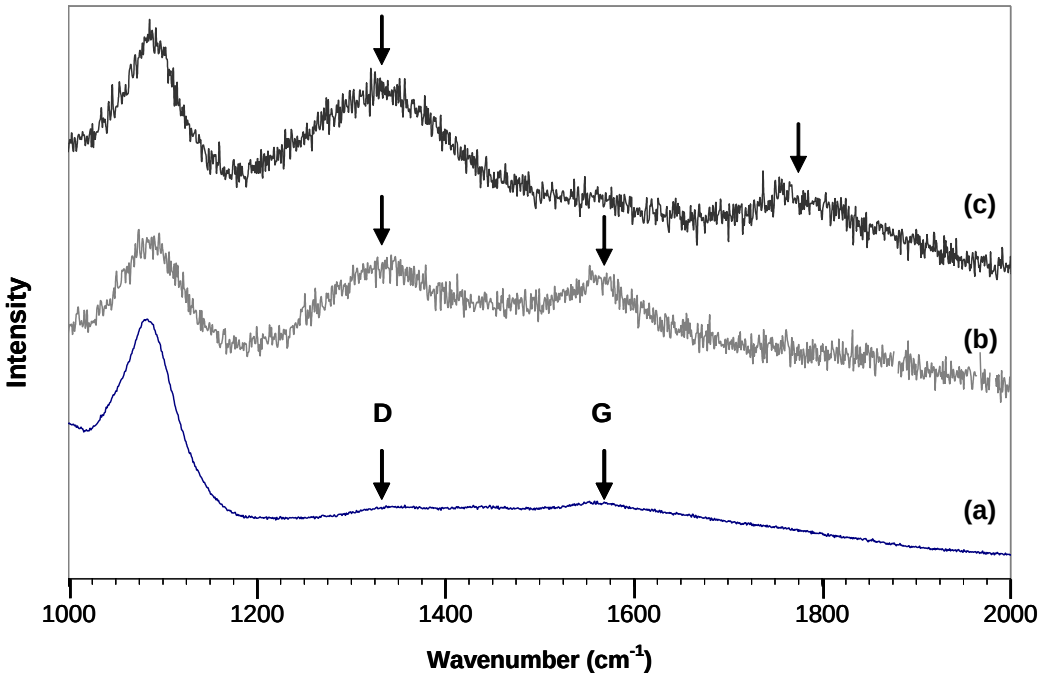

Figure 6. Raman spectra from B_4C cylinder impacted at 312 m/s. (a) Pristine region, (b) Shear localization band, and (c) Tip of shear localization band. Diode-based laser with excitation wavelength of 785 nm.

localization bands as indicated by arrows in Figure 5(c), become noticeable at the top of the eroded cone. While the bands can be described as irregular in shape, they appear to nominally follow the expected lines of maximum shear stress [11, 23]. Energy-dispersive spectroscopy revealed only B and C within the bands. Oxygen (O) was not detected. Figure 5(d) is a close-up of the fragments within a band. The fragments are clearly sub-micron in size, with the majority less than 0.5 μm in size (~ 100 nm). In their TEM examination of nanoindents in B_4C, Ge et al.[15] showed the presence of newly formed nano-crystals.

A basic question concerning these bands is whether or not the nano-scale shear amorphization mechanism, first observed by Chen et al.[13] and later by Ge et al.[15], is involved in their formation? In an attempt to answer this question, micro-Raman spectroscopy was used to determine if the material in these bands exhibit spectra consistent with shear amorphization.

Figures 6(a), (b), and (c) show the normalized Raman spectra for pristine B_4C, from within a shear localization band, and from the tip of the shear localization band, respectively. The relatively small D (disordered, ~ 1330 cm^{-1}) and G (graphite, ~ 1580 cm^{-1}) bands within the Raman spectrum for pristine B_4C most likely correspond to the

presence of very fine-scale intragranular disordered graphite (not the large graphite particles shown in Figure 3) [14, 24]. The Raman spectrum from the shear localization band indicates an increase in very fine-scale disordered graphite (relatively large D and G peaks), while that from its tip indicates very fine-scale amorphous C (large D peak coupled with almost non-existent G peak) [16]. In addition, the peak near 1780 cm^{-1} in the spectrum from the tip of the shear localization band has been previously attributed to the presence of amorphous B_4C (a-B_4C) [15, 25]. While these results are preliminary and additional work needs to be done in order to identify the mechanisms responsible for the spectra shown in Figures 6(b) and 6(c), they are consistent with the hypothesis that the shear amorphization mechanism is the precursor for the formation of the observed shear localization bands. That is, nano-scale shear amorphization ahead of the micro-scale shear localization band results in the formation of a-B_4C; subsequent deformation leads to fine-scale fragmentation of the a-B_4C into relatively narrow bands.

SUMMARY

In an attempt to gain better insight into the mechanisms responsible for both the ballistic and dynamic behaviors of B_4C, three cylinders of a commercial armor-grade B_4C variant were impacted with WC-6Co spheres at 103, 209, and 312 m/s, respectively. Sub-surface damage features were described. Examination of the impact site of the B_4C cylinder impacted at 312 m/s by FE-SEM revealed intense cracking and shear localization bands (i.e. inhomogeneous deformation). The material within these bands was finely comminuted. The apparent size of the B_4C fragments was sub-micron, with the majority of fragments less than 0.5 μm. Micro-Raman spectroscopy was used in an attempt to determine if shear amorphization was a possible mechanism for the formation of the bands by determining the nature of the fragments within the bands. The preliminary Raman spectra from a band and near its tip revealed features previously attributed to amorphization of B_4C. This supports the hypothesis that the formation of the shear localization bands is intimately connected with shear amorphization originally observed by Chen et al.[13] and mechanistically described by Fanchini et al.[16].

REFERENCES

1. R.C. Laible, “Ceramic Composite Armor,” Ballistic Materials and Penetration Mechanics, ed. R.C. Laible, Elsevier, New York, 1980, 135-143.
2. B. Matchen, “Applications of Ceramics in Armor Products,” *Key Eng. Mat.*, **122-124** 333-42 (1996).
3. H.-J. Ernst, V. Wiesner, and T. Wolf, “Armor Ceramics Under High-Velocity Impact of a Medium-Caliber Long-Rod Penetrator,” Ceramic Armor Materials By Design, eds. J.W. McCauley, A. Crowson, W.A. Gooch, A.M. Rajendran, S.J. Bless, K.V. Logan, M.J. Normandia, and S. Wax, *Cer.*

Trans., **134**, 23-31 (2002).
4. C.J. Roberson, P.J. Hazell, P.L. Gotts, I.M. Pickup, and R. Morrell, "The Effective Hardness of Hot-Pressed Boron Carbide with Increasing Shock Stress," *Cer. Eng. Sci. Proc*., **26** [7] 151-159, (2005).
5. D.E. Grady, "Shock-wave strength properties of boron carbide and silicon carbide," *J. Phy IV*, **C8** 385-390 (1994).
6. D.E. Grady, "Shock compression of brittle solids," *Mech. Mat*., **29**, 181-203 (1998).
7. N.K. Bourne, "Shock-Induced Brittle Failure of Boron Carbide," *Proc. R. Soc. Lond. A*, **458** 1999-2006 (2002).
8. D. P. Dandekar, "Shock Response of Boron Carbide," U.S. Army Research Laboratory, Report No. ARL-TR-2456 (2001).
9. T.J. Vogler, W.D. Reinhart, and L.C. Chhabildas, "Dynamic Behavior of Boron Carbide," *J. Appl. Phys*., **95** [8] 4173-4183 (2004).
10. A.S. Argon, "Mechanisms of inelastic deformation in metallic glasses," *J. Phys. Chem. Solids*, **43** [10] 945-961 (1982).
11. L. Anand and C. Su, "A theory for amorphous viscoplastic materials undergoing finite deformations, with application to metallic glasses," *J. Mech. Phys. Solids*, **53** 1362-1396 (2005).
12. T.J. Moynihan, J.C. LaSalvia, and M.S. Burkins, "Analysis of Shatter-Gap Phenomenon in a Boron Carbide/Composite Laminate Armor System," 20th International Ballistics Symposium, v2 Terminal Ballistics, eds. J. Carleone and D. Orphal, DEStech Publications, Lancaster, Pennsylvania, 2002, 1096-1103
13. M. Chen, J.W. McCauley, and K.J. Hemker, "Shock-Induced Localized Amorphization in Boron Carbide", *Sci*., **299** [5612] 1563-1566 (2003).
14. V. Domnich, Y. Gogotsi, M. Trenary, and T. Tanaka, "Nanoindentation and Raman spectroscopy studies of boron carbide single crystals," *Appl. Phys. Letters*, **81** [20] 3783-3785 (2002).
15. D. Ge, V. Domnich, T. Juliano, E.A. Stach, and Y. Gogotsi, "Structural Damage in Boron Carbide Under Contact Loading," *Acta Mat*., **52** 3921-3927 (2004).
16. G. Fanchini, J.W. McCauley, and M. Chhowalla, "Behavior of Disordered Boron Carbide under Stress," *Phys. Rev. Letters*, **97** 035502 (2006).
17. J.C. LaSalvia, M.J. Normandia, H.T. Miller, and D.E. MacKenzie, "Sphere Impact Induced Damage in Ceramics: I. Armor-Grade SiC and TiB_2," *Cer. Eng. Sci. Proc*., **26** [7] 171-179, (2005).
18. J.C. LaSalvia, M.J. Normandia, H.T. Miller, and D.E. MacKenzie, "Sphere Impact Induced Damage in Ceramics: II. Armor-Grade B_4C and WC," *Cer. Eng. Sci. Proc*., **26** [7] 180-188, (2005).
19. G.E. Hauver, E.J. Rapacki, P.H. Netherwood, and R.F. Benck, "Interface Defeat of Long-Rod Projectiles by Ceramic Armor", ARL Technical Report, ARL-TR-3590, September 2005, 85 pp.
20. M.A. Meyers, V.F. Nesterenko, J.C. LaSalvia, and Q. Xue "Shear Localization in Dynamic Deformation of Materials: Microstructural Evolution and Self-Organization," *Mat. Sci. Eng*., **A317** 204–225 (2001).
21. J. Swab, U.S. Army Research Laboratory, unpublished data.
22. M.J. Normandia, "Impact Response and Analysis of Several Silicon Carbides," *Int. J. Appl. Cer. Tech*., **1** [3] 226-234 (2004).
23. R. Hill, The mathematical theory of plasticity, Oxford University Press, New York, 1985, 355 pp.
24. M.W. Chen, J.W. McCauley, J.C. LaSalvia, K.J. Hemker, "Microstructural Characterization of Commercial Hot-Pressed Boron Carbide Ceramics," *J. Am. Cer. Soc*., **88** [7] 1935-1942 (2005).
25. X.Q. Yan, W.J. Li, T. Goto, and M.W. Chen, "Raman spectroscopy of pressure-induced amorphous boron carbide," *Appl. Phys. Letters*, **88** 131905 (2006).